Article

JOURNAL OF
biomaterials
applications

Journal of Biomaterials Applications
27(3) 241–254

DOI: 10.1177/0885328211401056
jba.sagepub.com
SAGE

Binary system thermodynamics to control pore architecture of PCL scaffold via temperature-driven phase separation process

Vincenzo Guarino[1], Angela Guaccio[2], Daniela Guarnieri[2], Paolo A Netti[2] and Luigi Ambrosio[1]

Abstract

The use of scaffold-aided strategies for the regeneration of biological tissues requires the fulfilment of an accurate architectural design, that is, micro and macrostructure, with the final goal of realizing architectures to adopt as guidance for those cell activities specific to the formation of novel tissues. Here, highly porous scaffolds made up of biodegradable poly(ε-caprolactone) (PCL) have been realized by thermally induced phase separation (TIPS). Two different polymer/solvent systems, derived by the dissolution of PCL in dioxane and DMSO respectively, were investigated. The aim was to demonstrate the high potential of TIPS technique, in imprinting specific pore features to the polymer matrices, by a conscious selection of polymer/solvent systems. The investigation of pore architecture by SEM/mercury intrusion porosimetry/image analyses, firstly allow to detect remarkable variations in porosity (from 92% to 78%,) and pore sizes, ranging from micro-scale (*ca* 10 μm) to macro-scale (greater than 100 μm) as a function of the used polymer/solvent systems. Moreover, experimental and theoretical evidences referred to scaffold shaped in custom-made molds – a thin Teflon ring between two copper plates – allow exploring how the sensitivity of polymer solution features (i.e., crystallinity, thermal inertia) to the cooling temperature can affect the alignment of polymer phases and, ultimately, scaffold pore anisotropy. Analytical results supported by preliminary biological studies demonstrate the higher ability of PCL/dioxane solution to promote the formation of aligned pores which provide a morphological guidance to cell advance during the preliminary stage of culture. These findings, taken as a whole, put the basis for a better informed regeneration of structurally complex tissues based on the modeling of scaffold micro and macro-architecture by thermodynamic forces.

Keywords

Scaffolds, phase separation, polycaprolactone, porosity, tissue engineering

Introduction

A significant challenge in current tissue engineering research is the capability to design polymer-based porous scaffolds with finely tuned pore morphology, which could effectively serve as a temporary morphological guide in the process of tissue and organ regeneration.[1–3] Nowadays, it is widely recognized that cell guidance by the scaffold requires a complex balance between chemical, biochemical, and biophysical cues, the goal being to reproduce the spatial and temporal microenvironments of the natural extracellular matrix.[4] In this context, it is known that the regeneration of tissues strongly depends on scaffold microarchitectural features, such as surface-to-volume ratio, pore size, and interconnectivity. For instance, it has been

[1]Institute of Composite and Biomedical Materials, National Research Council of Italy (IMCB/CNR), Piazzale Tecchio 80 Napoli, Italy
[2]Interdisciplinary Research Centre on Biomaterials CRIB, University of Naples, Piazzale Tecchio 80, 80125 Naples, Italy

Corresponding author:
Vincenzo Guarino, Institute of Composite and Biomedical Materials – National Research Council of Italy, Piazzale Tecchio 80, 80125 Naples, Italy.
Email: vguarino@unina.it

demonstrated that different tissues require different pore sizes for their regeneration, and that the diameter of cells in suspension dictates the minimum pore size, which varies as a function of cell type.[5] Recently, *in vitro* and *in vivo* studies suggested that scaffolds characterized by different pore size scales may improve the process of new-tissue regeneration by influencing cell morphology, cell binding, and phenotypic expression, as well as nutrient diffusion and tissue in-growth.[6]

Notably, the success of any tissue engineering scaffold-based strategy tends towards tissue biomimesis in terms of structural integrity. This is often in conflict with the need to maximize pore surface-to-volume ratio in order to enhance cell colonization and fluid transport. This conflict imposes a compromise between the adequate selection of materials and process technologies.[7,8] The use of a biocompatible/bioresorbable materials, with controllable degradation and resorption plus adequate mechanical properties, enables its optimal matching with the functional features of the tissue at the site of implantation.[9–12]

Biocompatible and biodegradable polymers, like aliphatic polyesters (i.e. polylactic acids, polyglycolic acids, and polycaprolactone), have great potential as supports for cell transplantation in the context of tissue repair and reconstruction.[13] This is in part due to their release of low molecular weight degradation products, such as lactic acid, which may enter the metabolic pathways and so directly affect cellular activities.[14] Since these degradation processes are now well known, it is possible to finely tune the resorption rate to match cell/tissue growth *in vitro* and/or *in vivo*.[11] However, poor processability and unsatisfactory biochemical and mechanical properties have restricted their use in tissue engineering.[15]

To overcome such limitations, temperature-driven processes, based on highly predictable procedures, have been implemented to develop polymer scaffolds for research studies[16] as well as large scale production. In particular, thermally driven phase separation represents an interesting approach for the preparation of polymer based scaffolds with encoded morphological and functional requirements.[10,17,18]

In the present article, highly porous poly(ε-caprolactone) (PCL) scaffolds, *via* a solid–liquid phase separation achieved by imposing a constant temperature drop, down to 4°C and −18°C respectively, on two different solvent/polymer binary systems, have been investigated. As previously reported in the literature, this process provides the physical separation of a polymer solution into two distinct phases, both with a globular aspect, and the later extraction of the solvent-rich phase, which leaves a porous structure with pores of micrometric sizes.[17]

However, an accurate definition of pore architectural features requires a sage evaluation of the thermodynamic forces involved in the phase separation mechanisms to establish the cooling modalities able to induce controlled demixing process[16] and crystallization.[18] Here, we demonstrate that PCL/dioxane and PCL/dimethylsulfoxide (DMSO) binary systems, because of their different thermodynamic affinity, can differently separate under similar cooling conditions, thus creating a various set of pore architecture in terms of size, interconnectivity, and pore anisotropy. Hence, we conclude that thermally induced phase separation (TIPS) process is a really tunable process and identifies an interesting route to design polymeric scaffolds able to induce the required biological recognition by controlling the morphological signal through the pore features.

Materials and methods

Materials

Scaffolds were obtained from polymer solution of polycaprolactone (PCL) (Sigma Aldrich M_w 65 kDa) dissolved into 1-4 dioxane (Sigma Aldrich, Italy) or DMSO (Sigma Aldrich, Italy). PCL is a semi-crystalline polymer with a melting temperature T_m of 57°C and a glass transition temperature T_g of −62°C. The solvents are highly volatile and present a freezing point respectively of 11.8°C and 18.2°C.[4]

Scaffold preparation

PCL was dissolved in 1-4 dioxane and DMSO respectively, at three different concentrations, 5, 10, and 15% w/w. PCL/dioxane solutions were prepared by magnetic stirring at room temperature for 90 min, while PCL/DMSO solutions at 50°C for about 8 h. When the total dissolution of both the components was achieved, after equilibration at room temperature, PCL solutions were poured into a TEFLON mold, 50 mm as diameter, and were frozen at 4°C and −18°C for 12 h; Subsequently, solutions were introduced into freeze dryer in order to induce the sublimation of solvent under vacuum (0,5 Torr) for 3 days, as function of solvent used, respectively, at 10°C for dioxane and 15°C for DMSO solutions. To create anisotropic scaffolds, tailored TEFLON molds comprising a double metal plate with high thermal conductivity (e.g., copper) were used. This promotes the formation of thermal gradients during the cooling process able to uniaxially direct the pore formation. Dish-shaped samples with thickness of 4 mm and diameter of 50 mm were prepared.

Pore morphology

SEM investigation: Different methodologies were used to investigate the pore architecture. Firstly, microstructure overview was performed by Scanning electron microscopy (SEM) of scaffold surfaces (Stereoscan 440 – Leica Oxford, UK). Previously, samples were gold-coated using a sputter coated set at 15 mA for 20 min in order to improve the surface conductivity and, as a consequence, the image quality. The qualitative SEM investigation allows monitoring the scaffold reproducibility by different batches as well as helps to determine pore features such as size, spatial distribution, and interconnectivity.

Estimation of scaffold porosity: Therefore, scaffold porosity and bulk density were also measured by gravimetric method at room temperature.[19] The density and the porosity of different porous structures were determined by measuring the dimensions and the mass of the scaffold. The density of the porous scaffold was calculated as follows:

$$d = \frac{m}{V'}$$

where m is the mass and V' is the volume of the porous structure. Porosity, P, was evaluated as:

$$P = 1 - \frac{d}{d_p}$$

where d_p is the density of nonporous scaffold.[20]

Finally, the pore size distribution of each sample was determined by using a mercury intrusion porosimetry (Pascal 140/240, ThermoElectron, Italy). Cylindrical shape of pores and constant pressure were assumed. Moreover, a mercury surface tension of 480 mN/m and a contact angle of 141.3° were imposed for all measurements. This method enables simultaneously to calculate total porosity, average pore, and size distribution. Finally, this method also provides an estimation of material and scaffold densities – respectively apparent and bulk densities – to confirm the qualitative measurement output by gravimetric method. For all the porosity measurements, disk-shaped samples with 5 mm diameter and 3 mm thickness were used ($n = 5$).

Pore anisotropy by FFT Image processing: PCL scaffolds with pore anisotropy were investigated by the elaboration of SEM images via NIH free software, Image J v.3.7 whereas pore orientation was estimated by spectral analysis of grey level images. This technique identifies a 2D image as a function of spatially varying image brightness $f(x,y)$, whereas gray-scale levels indicate all fluctuations of $f(x,y)$.[21] When transforming the image in its power spectrum or spectral density by fast Fourier transform (FFT), different frequencies are represented as different distances from the origin, and different directions represent different orientation in the original image; moreover, the power at each location shows how much of that frequency and orientation is present in the image. More specifically, the frequency space representation of a structure with an orientation θ, consists of a pie-shaped wedge of points located on each side of the 2D power spectrum centre, at a distance which corresponds to the wavelength of the original image with the orientation $\theta + \pi/2$. As a consequence, the power spectrum represents a precise indication of the orientation degree of a structure. Here, the frequency spectra of scaffold pore architecture from PCL/DMSO and PCL/dioxane solution were analyzed.

Polymer/solvent affinity

Hansen solubility parameters: The thermodynamic affinity of polymer/solvent system has been evaluated by the comparison of solubility parameters defined as the square root of cohesive energy per unit of volume V.[22] Since solubility parameters are available for only a limited number of solvents and polymers, here, the Hansen group method has been considered. This allows to predict approximate solubility parameters by the sum of squares of three different parameters, named Hansen solubility parameters (HSP), associated to cohesive energies arising from dispersive, permanent dipole-dipole, and hydrogen bonding forces.[23] The values determined for the solvents here, have been compared with the PCL (10.35 $(Cal/cm^3)^{1/2}$)[24] in order to qualitatively estimate polymer solvent affinity (Table 1).

Solvent thermal properties by DSC analysis: Moreover, Differential Scanning Calorimetry by DSC (TA instruments, mod. TA2910) was performed on both solvents to measure characteristic temperatures of evaporation and crystallization by imposing a cooling history from 18°C to −50°C by a scanning rate of 2°C/min.

Prediction of cooling rate by theoretical model: The kinetics of cooling for PCL/dioxane and PCL/DMSO systems were estimated by the heat balance equation as

Table 1. Solubility parameters of solvents by the Hansen group methods.

Solvents	Solubility parameters $(Cal/cm^3)^{1/2}$
Dioxane	10.1
DMSO	11.9

Table 2. Physico-chemical parameters, heat transfer coefficient and cooling rates.

	μ (mPa s)	ρ (g/cm^3)	c_p (cal/°C/g)	k (W/m/K)	h (kcal/cm^2/°C/h)		Q (kcal/h)	
Dioxane	1.18[21]	1.027	0.40[25]	0.16[26]	3.6	3	2.2	0.9
DMSO	1.99	1.09	0.45	0.18[27]				
Temperature T (°C)		25			−18	4	−18	4

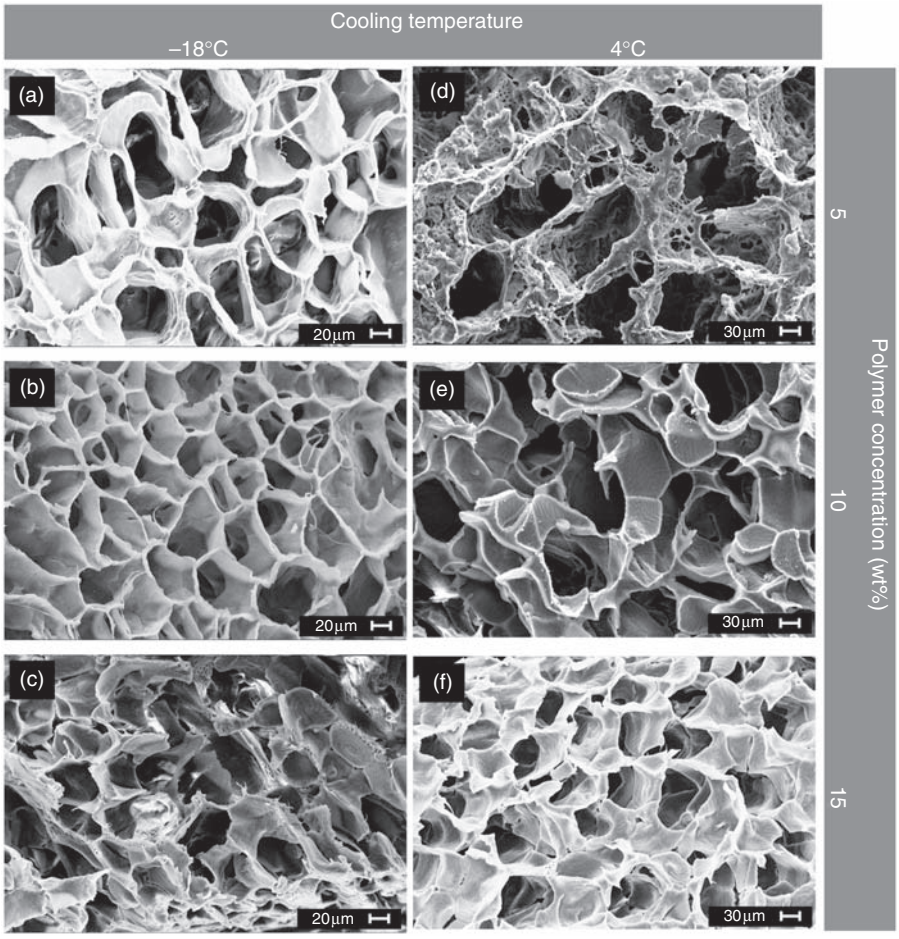

Figure 1. SEM image of scaffold surface from PCL/dioxane binary system at different polymer concentration – (a-d) 05/95, (b-e) 10/90, and (c-f) 15/85, under different cooling temperature: (a-b-c) −18°C and (d-e-f) 4°C.

follows. The heat transferred for unit time, Q, was derived by the equation:

$$m \cdot c_p \cdot \frac{dT}{dt} = -h \cdot S \cdot (T - T_a)$$

where h is the heat transfer coefficient, S is the characteristic exchange surface, T is the temperature of the system, and T_a the ambient temperature. In particular, at a first approximation, this was schematically represented as a problem of natural convection from a horizontal flat surface facing upward, so that any effect of variation in density and viscosity due to the phase transition was neglected. Moreover, the average heat transfer coefficients were calculated by the expression (Nusselt equation):

$$h = b \cdot \Delta T^m \cdot L^{3m-1}$$

where ΔT is $(T_f - T_m)$, T_f, the final cooling temperature equal to 4°C or −18°C, and T_m calculated as $(T_f + T_i)/2$ with $T_i = 25$°C. Noteworthy, b and m were related to the fluid properties while L referred to the geometry characteristic parameters.[21,25] These parameters were

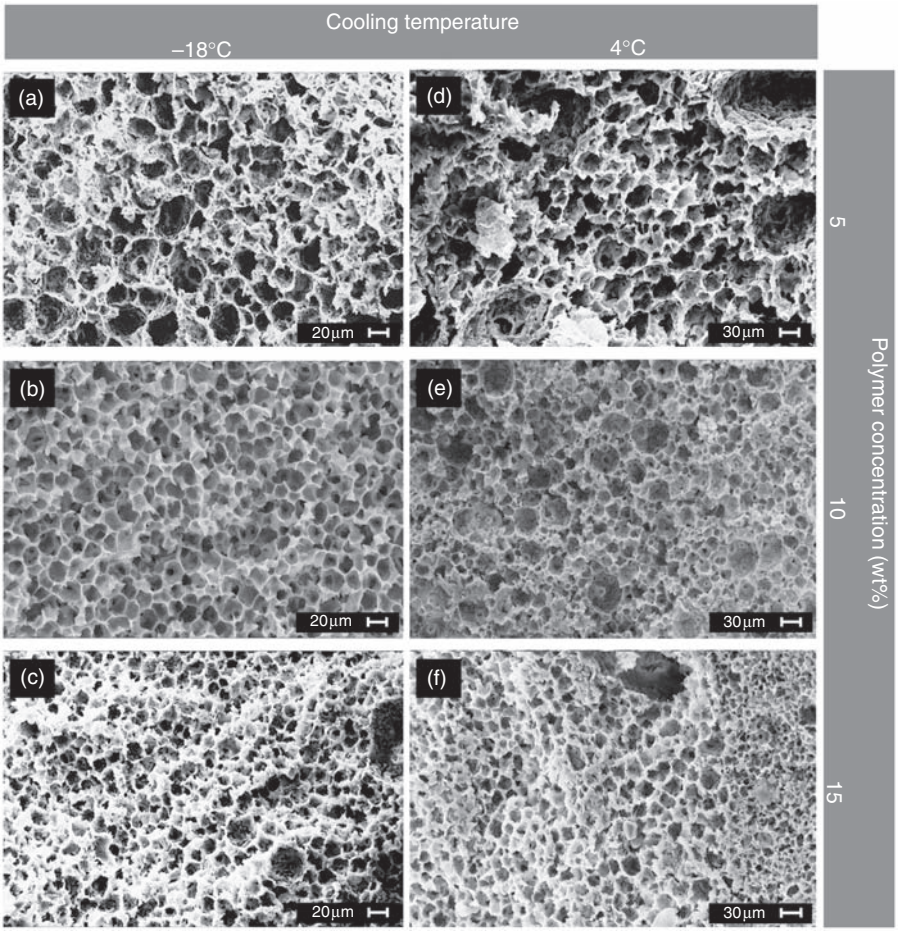

Figure 2. SEM image of scaffold surface from PCL/DMSO binary system at different polymer concentration: (a-d) 05/95, (b-e) 10/90, and (c-f) 15/85, under different cooling temperature: (a-b-c) −18°C and (d-e-f) 4°C.

calculated as a function of two dimensionless parameters, the number of Prandtl, *Pr*, and the number of Grashof, *Gr*, respectively. In the case of PCL/dioxane then PCL/DMSO systems, the product of these parameters falls in the range of $105 < Gr*Pr < 2*107$ (Table 2). Under these assumptions, b and m show the same value ($b = m = 1.86$), $m = ¼$, while L defined as the scaffold volume, and surface area ratio is equal to $D/4$, where D corresponds to the inner diameter of mold. The values of h and Q relative to both the systems are reported in Table 2.[26–29] The heat balance equation was integrated with a constant average h, m, and c_p to derive the time–temperature (t–T) diagram for dioxane and DMSO at 4°C and −18°C cooling temperature (Figure 1(a) and (b)).

Biological response

Cell culture: Bone marrow derived hMSCs (Clonetics, Italy), at the 5th passage, were cultured in α-Modified Eagle's medium (α-MEM) (Bio Wittaker, Belgium) containing 10% (v/v) FBS, 100 U/mL penicillin, and 0.1 mg/mL streptomycin (HyClone, UK) and, in a humidified atmosphere at 37°C and 5% CO_2. Before cell seeding, scaffolds were sterilized by antibiotic solution. About 5×10^4 cells, re-suspended in 50 μL of medium, were seeded on each scaffold and placed in 24-well culture plates (1 scaffold/well). After 2-h incubation at 37°C in a humidified atmosphere with 5% CO_2, 1.5 mL of fresh cell culture medium was added to each well. Cell/scaffold constructs were maintained in culture until 24 h. Cell viability experiments were conducted in triplicate and repeated at least three times.

Cell viability: Cell viability was evaluated by using the Alamar Blue assay (AbD Serotec Ltd, UK). The cell–scaffold constructs were removed from the culture plates after 1 day of culture, washed with PBS (Sigma–Aldrich, Italy), and placed into a new 24-well culture plate. For each sample, 1 mL of DMEM medium without Phenol Red (HyClone, UK) containing 10% (v/v) Alamar Blue reagent (working solution) was added, followed by incubation for 4 h at 37°C and 5% CO_2.

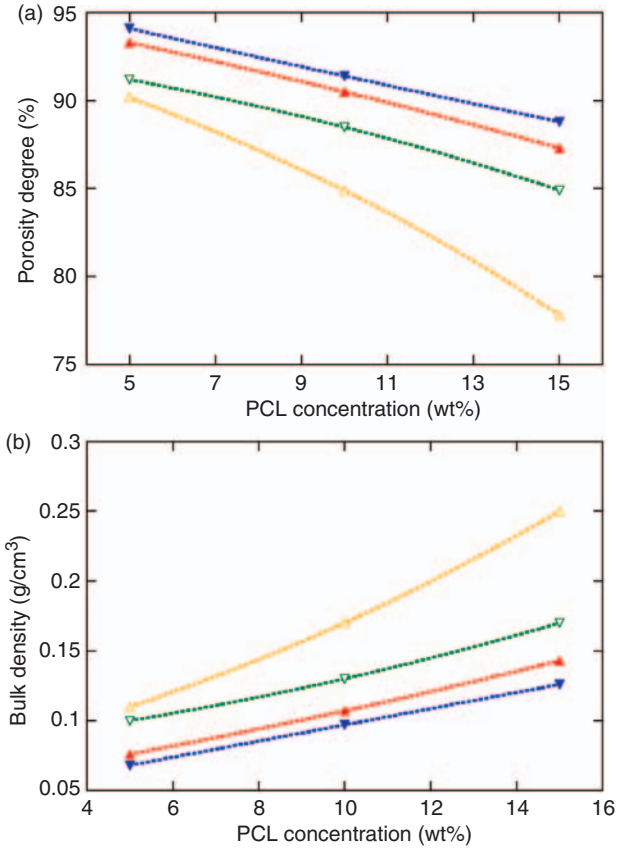

Figure 3. Porosity degree (a) and bulk density (b) assessment of different PCL binary systems by weight measurements: PCL/dioxane at 4°C (▲) or −18°C (▼) and PCL/DMSO at 4°C (△) or −18°C(▽).

About 1 mL of working solution was also added in a well w/o cells and used as control. The solution was subsequently removed from the wells and analyzed by a spectrophotometer (multilabel counter, 1420 Victor, Perkin Elmer, Italy) at wavelengths of 570 and 600 nm.

CLSM imaging: After 24 h of culture, the cell/scaffold constructs were fixed with 4% paraphormaldeyde for 20 min at RT, rinsed twice with PBS buffer and incubated with PBS-BSA 0.5% to block unspecific binding. Actin microfilaments were stained with phalloidin tetramethylrhodamine B isothiocyanate (Sigma-Aldrich, Italy). Phalloidin was diluted in PBS-BSA 0.5% and incubated for 30 min at RT. Cell nuclei were stained by using 4',6-Diamidino-2-phenylindole (DAPI) (Sigma-Aldrich, Italy). The DAPI stock solution (10 mg/mL in DMSO) was diluted in PBS ($1/10^4$ v/v) and incubated for 10 min at 37°C. The samples were then rinsed 3 times with PBS and observed by confocal laser scanning microscope (LSM510, Zeiss, Germany) equipped with a He-Ne laser, at a wavelength of 543 nm and objectives 10 ×.

Results

SEM images of PCL scaffolds prepared under different cooling temperatures, 4°C and −18°C, by dissolving three different PCL weight fractions, 5, 10, and 15 wt%, in dioxane (Figure 1) and DMSO (Figure 2) were reported. Comparing the micrographs at the same magnification, it results that morphology depends upon the polymer concentration, cooling temperature, as well as solvent used. Concerning PCL scaffold from dioxane solution, Figure 1 shows an open-cell porous structure with full interconnection among pores. Pore size remarkably varies as a function of the cooling temperature, while, only a slight effect on pore size seems to be ascribable to the PCL concentration. Contrariwise, PCL scaffolds from DMSO solution exhibit a honeycell porous structure with smaller pore size than the previous one at the same process condition. The pore architecture seems not to be significantly influenced by the polymer concentration and cooling modality.

The qualitative evaluation of scaffold porosity has been supported by an extensive estimation of porosity features by different experimental methodologies based on weight measurement and fluid intrusion techniques. Results obtained by the former methods are summarized in Figures 3 and 4. Data show that porosity is reduced as the polymer concentration increases, coherently with the solvent amount reduction (Figure 3). Some differences may be detected by the evaluation of porosity trends as a function of the solvent used. In particular, porous scaffolds from PCL/DMSO solution evidence lower porosity with values down to 77%, probably due to an underestimation of the total porosity, determined by the contribution of structural defects.

The request of more reliable and accurate measurements of porosity often implied the use of alternative techniques based on the fluid intrusion.[29–31] This technique is not able to detect closed pores, so allowing the sole evaluation of fully interconnected pore network.

Here, the evaluation of porosity was obtained by the estimation of pressure gradients which are forming as mercury fluid volume intrudes into the porous structures. Noteworthy, the measurements have not been compromised by the applied pressure,[32] with lacks of scaffold damages, as confirmed by density values (Table 3) in total agreement with values reported in the literature.[33] Here, the applied pressure is adapted to the sample material so achieving a complete screening of basic porosity parameters without measure artefacts. All the results are summarized in Table 3. They confirm trends in porosity previously obtained by gravimetric methods. In particular, lower values in porosities estimated for PCL/DMSO systems, may be due to the presence of closed pores which limit the

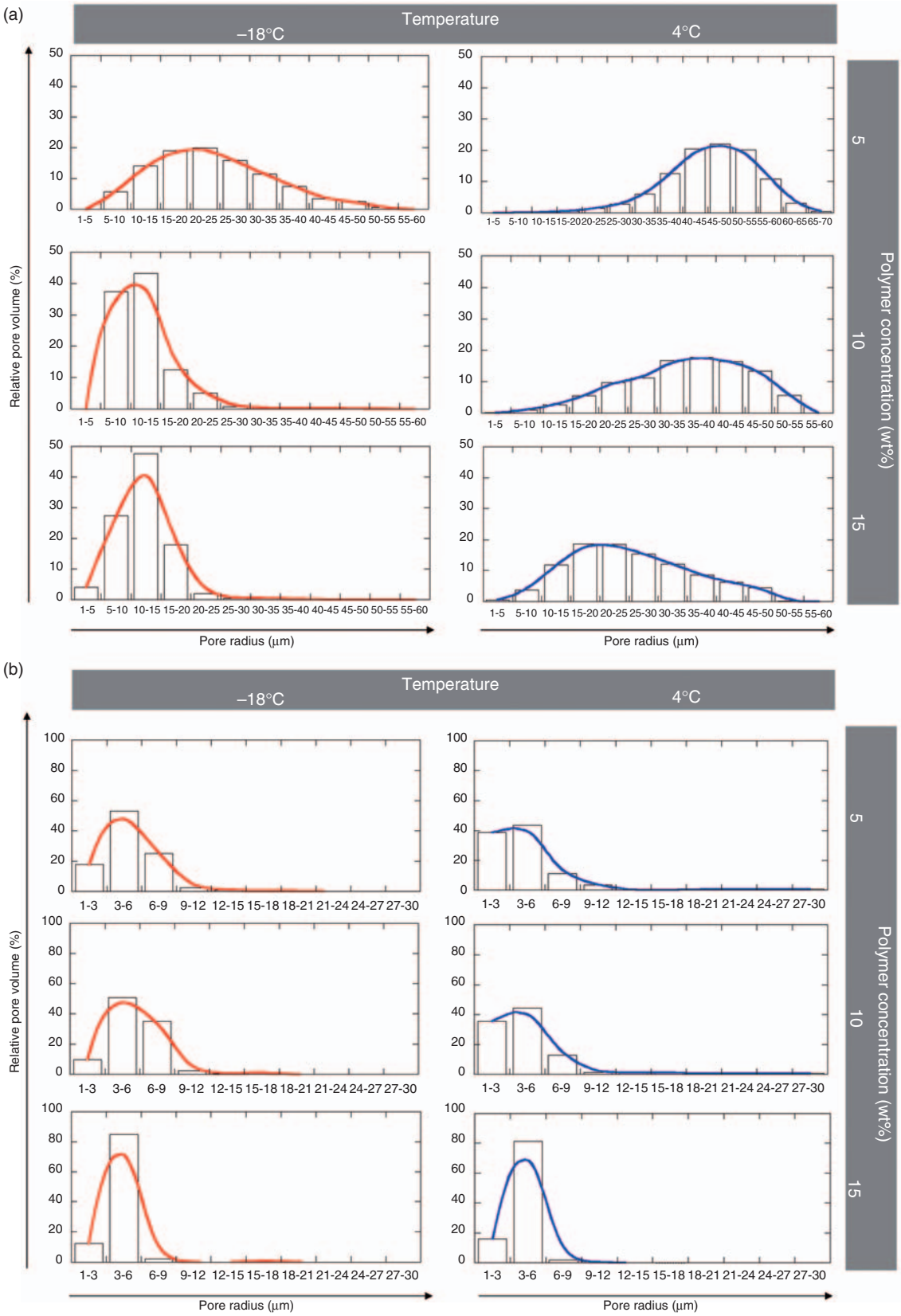

Figure 4. Pore size distribution by mercury intrusion porosimetry: (a) PCL/dioxane and (b) PCL/DMSO.

Table 3. Estimation of basic porosity features by mercury intrusion porosimetry.

Polymer concentration (wt%)	Cooling temperature (°C)	Solvent	Porosity (%)	Average pore radius (μm)	Bulk density (g/cm^3)	Apparent density (g/cm^3)	Total specific surface area (m^2/g)
5	−18	DMSO	80.5	5.44	0.21	–	1.76
5	4	DMSO	77.8	4.21	0.22	–	1.68
10	−18	DMSO	81.5	6.59	0.19	–	1.67
10	4	DMSO	78.2	4.45	0.23	–	1.63
15	−18	DMSO	79.8	3.38	0.22	–	1.91
15	4	DMSO	76.6	2.98	0.24	–	1.63
5	−18	Dioxane	91.7	25.6	0.09	1.16	0.986
5	4	Dioxane	84.6	55.3	0.15	1.10	0.477
10	−18	Dioxane	84.7	16.9	0.17	1.11	0.891
10	4	Dioxane	79.7	47.2	0.20	1.09	0.254
15	−18	Dioxane	78.3	13.1	0.24	1.12	0.627
15	4	Dioxane	76.5	30.5	0.27	1.13	0.280

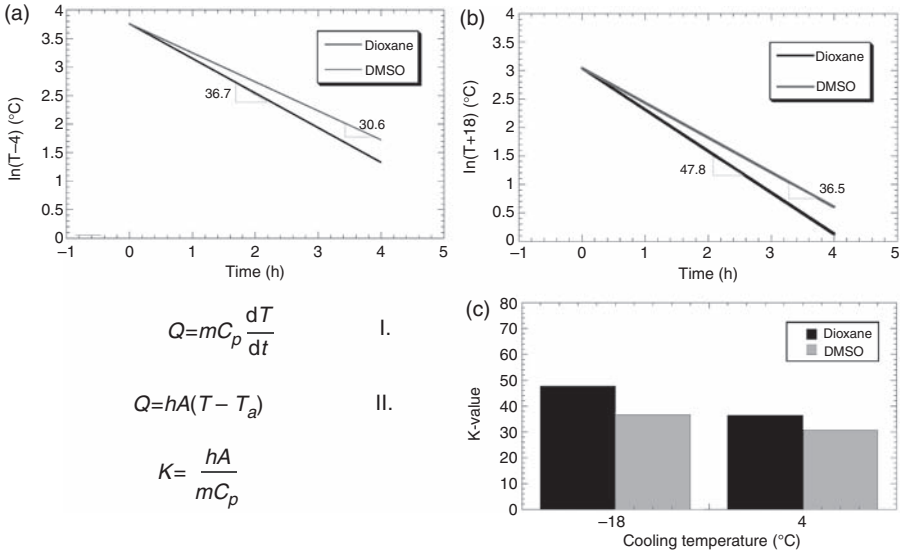

$$Q = mC_p \frac{dT}{dt} \quad \text{I.}$$

$$Q = hA(T - T_a) \quad \text{II.}$$

$$K = \frac{hA}{mC_p}$$

Figure 5. Temperature vs time diagrams at 4°C (a) and −18°C (b) cooling temperature, for dioxane and DMSO systems; heat balance equation, parameters definition and slope of the cooling curves (c).

penetration of mercury within the porous structure. Pore size estimation is in total agreement with SEM evidences. Pore measurements confirm a slight variation of pore radius in the case of PCL/DMSO system ranging from 2.98 to 6.59 μm, whereas more relevant differences were underlined in the case of PCL/dioxane with pore radii ranging from 16.9 to 55.3 μm. These differences are also confirmed by values of total pore surface which show higher values in the case of PCL/DMSO system, ascribable to smaller pore sizes of the scaffold. Furthermore, pores are also characterized by a broad distribution of sizes as clearly reported in Figure 4. Moreover, distribution curves show a left-shift moving towards lower temperatures and higher concentrations in the case of PCL/dioxane system (Figure 4(a)). Contrariwise, not relevant curve shift may be recognized in the case of PCL/DMSO systems (Figure 4(b)).

Thermodynamic affinity of PCL in dioxane or DMSO solution has been evaluated by the calculation of solubility parameters, summarized in Table 1. The solubility parameter of dioxane equal to 10.1 $(Cal/cm^3)^{1/2}$ results to be similar to the PCL value, so indicating that dioxane is a good solvent for PCL.

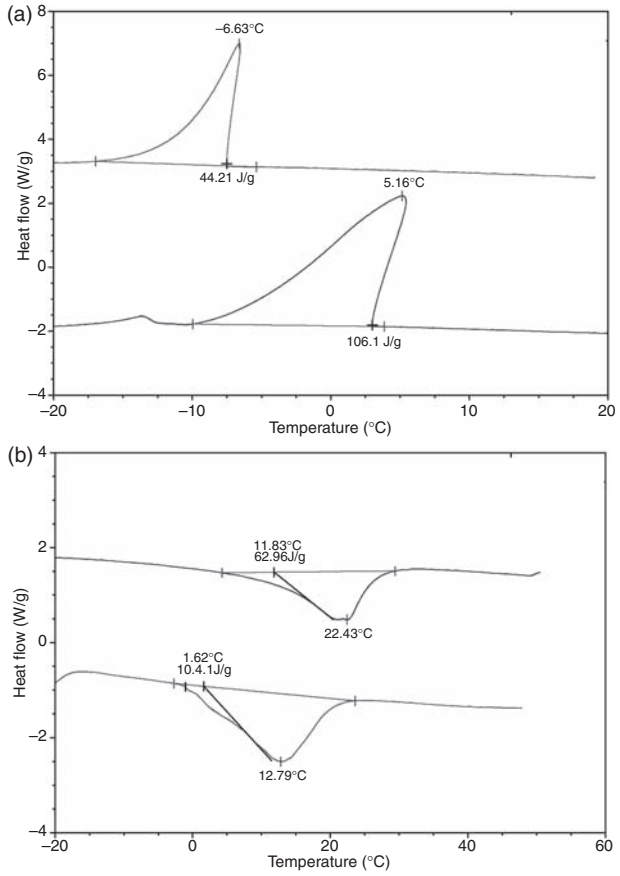

Figure 6. DSC thermograms: crystallization (a) and melting (b) points of DMSO (upper) and dioxane (down).

Contrariwise, DMSO shows a coefficient equal to 11.9 $(Cal/cm^3)^{1/2}$ which explains the poor affinity with the polymer. Moreover, to elucidate the effect of cooling rate on scaffold morphology, heat balance equation for binary systems (see Materials and methods section) has been used. Data derived by the solution of the heat balance equation show that, at 4°C cooling temperature, the difference between the cooling rates in dioxane and DMSO systems is slightly remarkable (Figure 5(a)), i.e., the effect of solvents on the kinetics of the process is negligible, as confirmed by the slopes of the cooling curves (Figure 5(c)). Conversely, at −18°C cooling temperatures, cooling curves show different slopes, indicating a higher cooling rate for dioxane system, with $K = 47.8$ (Figure 5(b) and (c)).

At the same time, a lower crystallization temperature of DMSO (−6.82°C) respect to dioxane (5.18°C), has been detected by DSC thermograms (Figure 6), so remarking the higher thermal inertia of DMSO which tend to hinder the growth of crystalline structures. As a consequence, Teflon molds with conductive components which allow to uniaxially control thermal gradient along the scaffold thickness, were used to amplify the differences in pore architecture due to the thermal properties of polymer solutions (Figure 7). Under stronger cooling (−18°C), PCL/DMSO systems form rounded pores (Figure 7(b)–square) whereas PCL/dioxane system originates a pore architecture with microtubular channels (Figure 7(a)–square) which were organized into domains oriented along the thermal gradient as extensively reported by several authors.[34,35] In this case, the use of copper plates forces the thermal gradient to occur perpendicularly to the plates, so resulting in the formation of densely packed vertical arrays of dioxane crystals. However, this characteristic pore architecture is not detected for scaffolds prepared at 4°C, which also showed the presence of spherical pores (data not shown). From the cross sectional view (Figure 7(a)–square), it has been recognized that an array of straight parallel channels from 10 to 60 μm in diameter go across the entire scaffold thickness, where on the scaffold surface round shaped pores have been detected (Figure 7(a)). Different pore anisotropy has been also evaluated by image processing techniques on selected SEM images. Figure 7(c) and (d) show the FFT-derived power spectra from SEM micrographs of PCL/dioxane and PCL/DMSO scaffolds. As expected, the former power spectrum (Figure 7(c)) individuates a pattern oriented along a direction individuated by angle θ greater than π/2 (square), corresponding to SEM images in which most pore edges are perpendicularly oriented (Figure 7(a)). In contrast, the power spectrum for the SEM morphology from PCL/DMSO solution is rather isotropic, with all the excited frequencies distributed in a central circle and surrounded by a halo of decreasing density (Figure 7(d)).

Scaffolds with different pore size and anisotropy have been preliminary tested under cell culture to validate the biological response of the proposed systems. Figure 8 shows that hMSCs cells well adhere and spread on both PCL/DMSO and PCL/dioxane scaffolds. In particular, Alamar Blue assay data (Figure 8) show that hMSCs cells are adhered and viable after 24 h of culture on both the scaffold typologies, indicating a good cell-material interaction (Figure 8). Moreover, no significant differences in cell viability were observed between PCL/DMSO and PCL/dioxane scaffolds. However, only few changes in cell shape, detected by cytoskeleton staining, may be correlated to the differences in pore size and morphology. In particular, on PCL/dioxane scaffolds, cells appear more stretched and oriented along the characteristic scaffold channels (Figure 8(b)). Conversely, in PCL/DMSO scaffolds with smaller pore without preferential orientation, cells appear randomly distributed, with tendency of forming clusters on the scaffold surface (Figure 8(c)), probably due to the limited cell penetration determined by the reduced pore size.

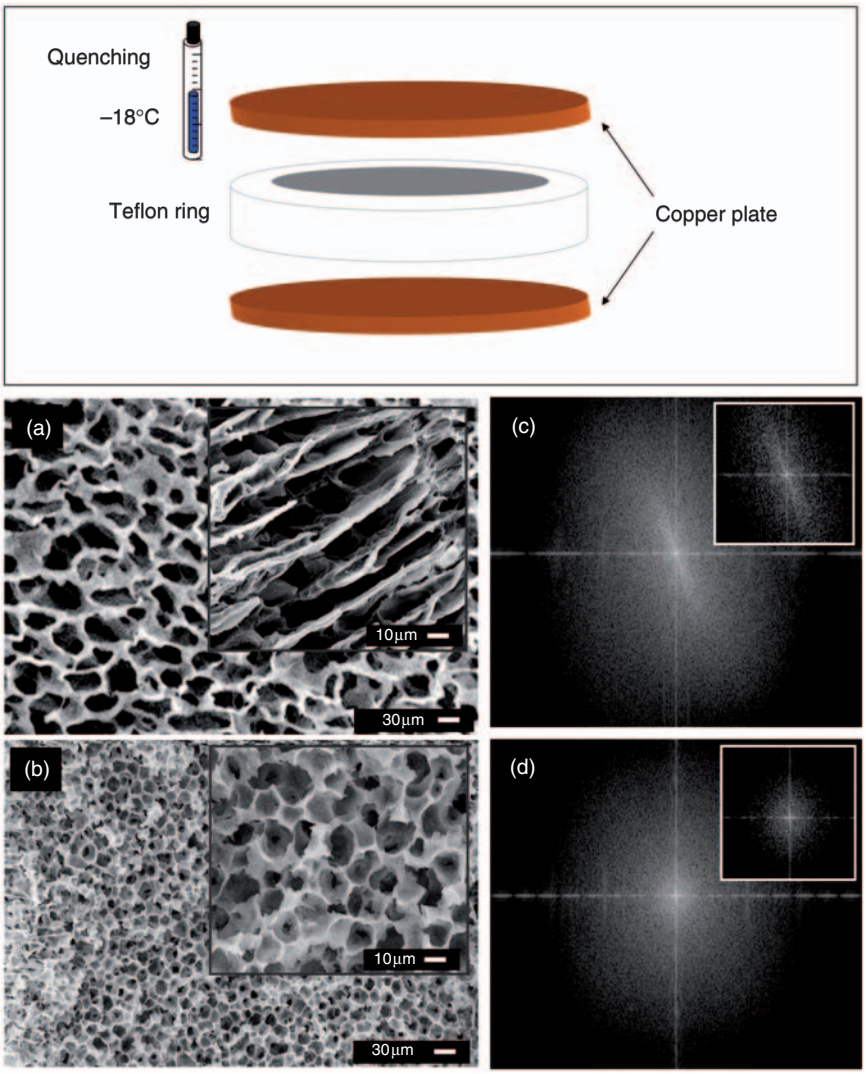

Figure 7. Different pore anisotropy of scaffold prepared in Teflon mold covered by copper plates from PCL/DMSO (a-c) and PCL/dioxane (b-d) solution. (a-b) SEM images of scaffold surface – in the square, cross section at higher magnification were reported; (c-d) FFT spectra of scaffold cross section.

Discussion

The fabrication of polymer scaffolds through a temperature-driven phase separation approach has been extensively studied[36] to design 3D platforms with tailored pore architectural features including porosity, pore size, surface area-to-volume ratio, interconnectivity, anisotropy, and strut thickness. By this experimental route, the pore architecture of scaffold can be designed by guiding the mechanisms of thermodynamic-driven separation of polymer/solvent binary systems – phase nucleation and growth – occurring between binodal and spinodal regions.[37] Indeed, these mechanisms are mainly controlled by the peculiar thermodynamic forces which govern the microscopic interaction between polymer and solvent components,[38] the same that influence selective macromolecular events (i.e., polymer gelation or solvent crystallization). So far, such events are strictly dependent on the polymer/solvent binary system used, and can affect the final scaffold morphology.[39] As a consequence, the modulation of phase separation conditions allows to achieve various pore structures in terms of morphology, pore sizes, and pore distributions.

This study is aimed at investigating the different mechanisms of phase separation occurring in the case of two binary systems by the dissolution of PCL in dioxane and DMSO, respectively. It has been just demonstrated that dioxane is able to crystallize into different geometries depending on its concentration within

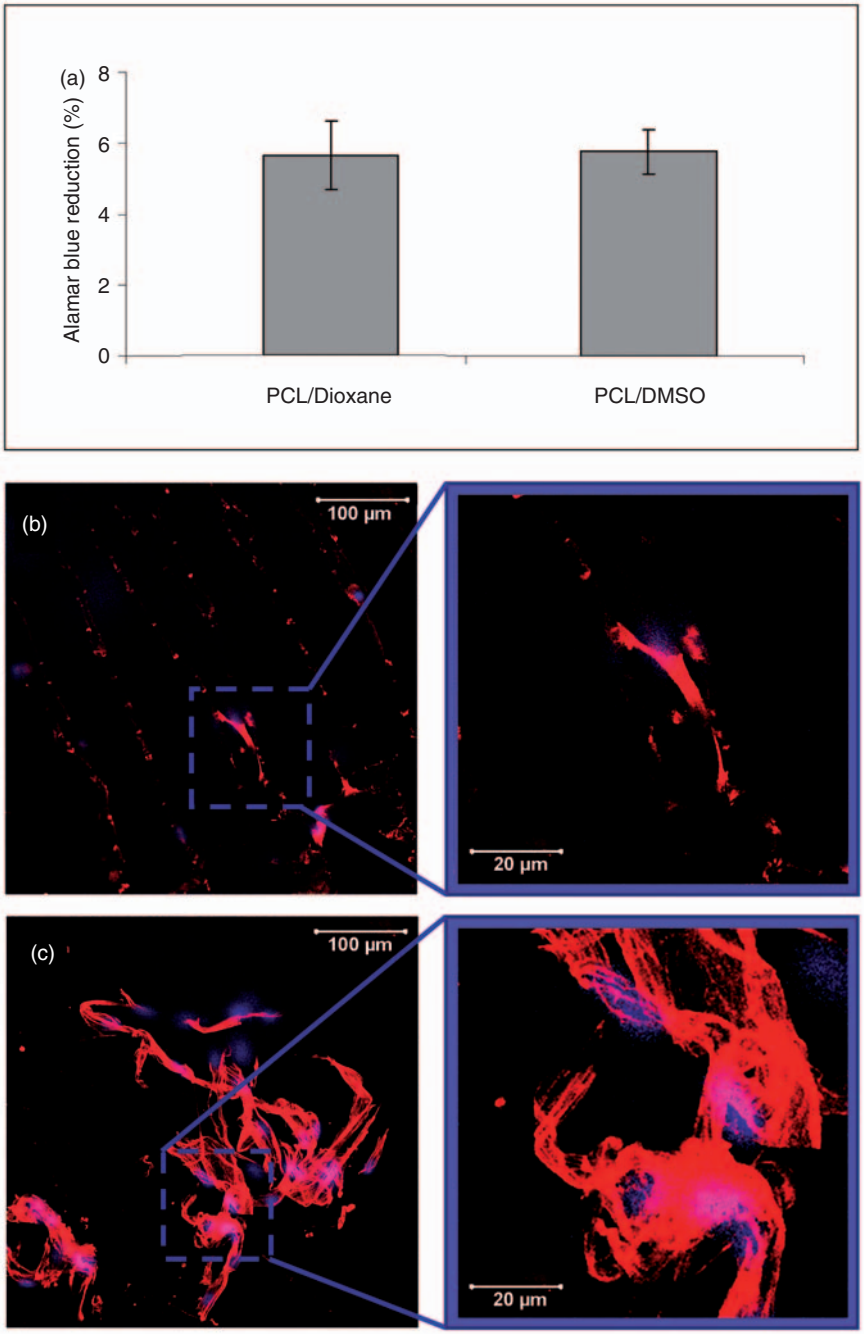

Figure 8. Biological assays on PCL scaffolds from different polymer/solvent solution. (a) Cell viability on scaffolds obtained by cooling at −18°C; (b-c) CLSM images of actin microfilaments (in red) and nuclei (in blue) of hMSCs cells grown on porous scaffolds obtained from PCL/dioxane (b) and PCL/DMSO (c) systems. Magnification 10 ×.

the polymer solution and quenching conditions.[40] The ability to control solvent shaping under solidification is crucial because crystallite geometry and order act as a template for porosity. Here, two different cooling temperatures, respectively 4°C and −18°C, both lower than the freezing point of both the proposed solvents, have been chosen to selectively induce solvent crystallization phenomena. PCL/dioxane systems, cooled down to 4°C, show active mechanisms of phase growth as confirmed by pores with bigger sizes (Figure 1(a)–(c)) whereas the quenching down to −18°C lock-in the phase nucleation at the beginning

of the cooling stage, and a fast crystallization of solvent occurs so that pores drastically decrease in size (Figure 1(d)–(f)). Moreover, increasing polymer concentrations as well as lower cooling temperatures drastically hinder the polymer chain mobility during the cooling process, so concurring to significantly affect the final size of phases/pores as extensively indicated by porosity measurements (Figures 3 and 4).

Conversely, a different pore morphology may be recognized in the case of binary PCL/DMSO systems (Figure 2), according to poor polymer/solvent affinity (Table 1) and higher thermal inertia (Figure 5), which affect phase formation mechanisms upon solidification. In particular, the higher melting point of the DMSO (Figure 5) implies higher ΔT of undercooling, so determining a predominant effect of nucleation mechanisms with respect to the phase growth, in turn, depending on the polymer concentration. Interestingly, the modeling of the heat transfer associated to the phase separation mechanism demonstrated a significant difference at -18°C cooling temperature, evidenced by the value of K, probably ascribable, again, to the different thermal inertia of solvent used (Figure 5). These data suggest that the morphological implications of the use of different solvents might be substantially ascribable to the thermodynamic features, which are function of the polymer/solution system properties. Besides, the mechanisms of solid–liquid phase separation in homogeneous semicrystalline polymer solutions, are more complex than liquid/liquid phase separation ones, since they have to take into account the competing kinetics of liquid/liquid separation and crystal formation. Generally, liquid/liquid phase separation and crystallization are highly sensitive to temperature, even though crystallization is dominant as the quenching temperature progressively decreases. As a consequence of different polymer/solvent interactions, carried by thermodynamic driving forces,[41,42] crystallization mechanisms can differently occur as the solvent changes with relevant effect on final pore morphology (Figures 7). Recent studies just demonstrated that the imposition of anisotropic thermal gradient to the polymeric solution can force dioxane crystallization along specific directions, ordering the whole system at a macroscopic level.[43] In this case, we test the tendency of two different polymer solution to form preferentially aligned crystals by using a custom-made mold composed of a thin Teflon ring covered by two copper plates. By imposing the same cooling rate (-18°C), DMSO solution with lower crystallization point shows a slower growth of solvent crystals which implies an architecture with globular pores. Conversely, dioxane solution with higher crystallization point shows a faster crystal growth, so promoting the characteristic dendrite-like pore morphology, extensively reported in the literature.[36,44]

The ability to modulate pore size and anisotropy has great value in scaffold design for tissue regeneration. Many tissues – such as nerve, muscle, blood vessel, tendon, ligament, dentin – are organized as hierarchical structures, comprising oriented tubular or fibrous bundle architectures.[20] Here, we preliminarily verified that these proposed scaffolds are distinctly recognized by hMSC cells, as indicated by their good viability after 24h. Moreover, CLSM images (Figure 8) show that cells better recognize aligned pore architecture, thus confirming the capability of pore anisotropy to influence cell adhesion. This result is in agreement with recent studies[43] on similar scaffolds which demonstrate that pore architecture drives cellular growth while also preserving their multi-potency towards differentiation. However, these results also remark the main shortcoming of the TIPS process concerning the limited capability of modulating pore sizes over 100 μm[16]. Confocal images on PCL/DMSO scaffolds clearly shows that pores, 20–30 μm in size, are too small to meet the optimal housing requirements of hMSC cells, thus compromising their use for tissue regeneration. In this context, the sage choice of materials and process parameters may drastically contribute to optimize the pore features such as pore size and alignment (Figure 8(b)). Besides, recent works demonstrated the successful use of TIPS scaffolds with pore sizes of ca. 100 μm in vascular tissue engineering through the support of cell dynamic seeding/culture methodologies.[43] In this case, the use of bioreactor systems allows forcing cells to more easily move into the porous network thus assuring a more homogeneous cell colonization of the 3D structure. Alternatively, the combination of TIPS techniques with traditional salt leaching may further contribute to the design of pore architecture by imparting a multi-scale porosity[45] – macropores and micropores together – able to enhance cell colonization as well as the molecular trafficking, thus morphologically and functionally supporting the growth of natural tissues.

Conclusion

Highly porous scaffolds made up of biodegradable PCL have been developed by temperature-driven phase separation of different polymer solutions. In this article, it has been shown that the properties of the solvent – here, dioxane or DMSO – play a key role in regulating the mechanism of phase separation. This in turn demonstrates the validity of temperature-driven phase separation techniques to implement tailored pore architectures with pore anisotropy for different applications in tissue engineering.

Acknowledgment

This study was supported from the Ministero dell'Universita' e della Ricerca by funds of Rete Nazionale di Ricerca TISSUENET n. RBPR05RSM2.

References

1. Bonassar LJ and Vacanti CA. Tissue engineering: the first decade and beyond. *J Cell Biochem* 1998; 72: 297–303.
2. Mikos AG, Thorsen AJ, Czerwonka LA, Bao Y, Langer R, Winslow DN, et al. Preparation and characterization of poly(L-lactic acid) foams. *Polymer* 1994; 35: 1068–1077.
3. Yang S, Leong KF, Du Z and Chua CK. The design of scaffolds for use in tissue engineering. Part I. Traditional factors. *Tissue Eng* 2001; 7: 679–689.
4. Ma PX and Zhang R. Microtubular architecture of biodegradable polymer scaffolds. *J Biomed Mater Res A* 2001; 56: 469–477.
5. Aronin CEP, Sadik KW, Lay AL, Rion DB, Tholpady SS, Ogle RC, et al. Comparative effects of scaffold pore size, pore volume, and total void volume on cranial bone healing patterns using microsphere-based scaffolds. *J Biomed Mater Res Part A* 2009; 89A: 632–641.
6. Madden LR, Mortisen DJ, Sussman EM, Dupras SK, Fugate JA, Cuy JL, et al. Proangiogenic scaffolds as functional templates for cardiac tissue engineering. *PNAS* 2010; 24: 15211–15216.
7. Andriano KP, Tabata Y, Ikada Y and Heller J. In vitro and in vivo comparison of bulk and surface hydrolysis in absorbable polymer scaffolds for tissue engineering. *J Biomed Mater Res* 1999; 48: 602–612.
8. Causa F, Netti PA and Ambrosio L. A multi-functional scaffold for tissue regeneration: the need to engineer a tissue analogue. *Biomaterials* 2007; 28: 5093–5099.
9. Harris LD, Kim BS and Mooney DJ. Open pore biodegradable matrices formed with gas foaming. *J Biomed Mater Res* 1998; 42: 396–402.
10. Laurencin CT, Ko FK, Attawia MA and Borden MD. Studies on the development of a tissue engineered matrix for bone regeneration. *Cell Mater* 1998; 8: 175–181.
11. Sachlos E and Czernuszka JT. Making tissue engineering scaffolds work. Review: the application of solid freeform fabrication technology to the production of tissue engineering scaffolds. *Eur Cell Mater* 2003; 5: 29–40.
12. Whang K, Goldstick TK and Healy KE. A biodegradable polymer scaffold for delivery of osteotropic factors. *Biomaterials* 2000; 21: 2545–2551.
13. Karande TS, Ong JL and Agrawal CM. Diffusion in musculoskeletal tissue engineering scaffolds: design issues related to porosity, permeability, architecture, and nutrient mixing. *Ann Biomed Eng* 2004; 32: 1728–1743.
14. Schugens C, Maquet V, Grandfils C, Jerome R and Teyssie P. Polylactide macroporous biodegradable implants for cell transplantation. II. Preparation of polylactide foams by liquid-liquid phase separation. *J Biomed Mater Res* 1996; 30: 449–461.
15. Rezwan K, Chen QZ, Blaker JJ and Boccaccini AR. Biodegradable and bioactive porous polymer/inorganic composite scaffolds for bone tissue engineering. *Biomaterials* 2006; 27: 3413–3431.
16. Guarino V and Ambrosio L. Temperature driven processing techniques for manufacturing fully interconnected porous scaffolds in bone tissue engineering. *P I Mech Eng H* 2010; 224: 1389–1400.
17. Ma PX. Scaffolds for tissue fabrication. *Mater today* 2004; 7: 30–40.
18. Zhang R and Ma PX. Poly(alpha-hydroxyl acids)/hydroxyapatite porous composites for bone-tissue engineering. I. Preparation and morphology. *J Biomed Mater Res* 1999; 44: 446–455.
19. Hou Q, Grijpma DW and Feijen J. Porous polymeric structures for tissue engineering prepared by a coagulation, compression moulding and salt leaching technique. *Biomaterials* 2003; 24: 1937–1947.
20. Hu Y, Grainger DW, Winn SR and Hollinger JO. Fabrication of poly(α-hydroxy acid) foam scaffolds using multiple solvent systems. *J Biomed Mater Res* 2002; 59: 563–572.
21. Russ JC. *The image processing handbook*. Boca Raton, FL: CRC press, 2006.
22. Hamedi M and Danner RP. Prediction of solubility parameters using the group-contribution, Lattice-Fluid Theory. *J Appl Polym Sci* 2001; 80: 197–206.
23. Hansen C. *Hansen solubility parameters: A user's handbook*, 2nd ed. Boca Raton, Fl: CRC Press, 2007.
24. Sarac A, Ture A, Cankurtaran O and Yilmaz F. Determination of some thermodynamical interaction parameters of polycaprolactone with some solvents by inverse gas chromatography. *Polym Int* 2002; 51: 1285–1289.
25. Perry RH and Green DW. *Perry's chemical engineers handbook*. New York: McGraw-Hill, 1997.
26. Lorenzi L, Fermeglia M and Torniano GJ. Densities and viscosities 1,1,1-trichloroethane with 13 different solvents at 298.15 K. *J Chem Eng Data* 1995; 40: 1172–1177.
27. Grolier JPE, Roux-Desgranges G, Berkane M, Jiménez E and Wilhelm EJ. Heat capacities and densities of mixtures of very polar substances 2.Mixtures containing N,N-dimethylformamide. *J Chem Thermodyn* 1993; 25: 41–50.
28. Van Asten AC, Kok WT, Tijssen R and Poppe H. Study of thermal diffusion of polybutadiene and polytetrahydrofuran in various organic solvents. *J Polym Sci Pol Phys* 1996; 34: 297–308.
29. Zhang HF, Zhao G, Ye H, Ge XS and Cheng SX. An improved hot probe for measuring thermal conductivity of liquids. *Meas Sci Technol* 2005; 16: 1430–1435.
30. Shi G, Cai Q, Wang C, Lu N, Wang S and Bei J. Fabrication and biocompatibility of cell scaffolds of poly(L-lactic acid) and poly(L-lactic-co-glycolic acid). *Polym Adv Technol* 2002; 13: 227–232.
31. Luetzow K, Klein F, Weigel T, Apostel R, Weiss A and Lendlein A. Formation of poly(epsilon-caprolactone) scaffolds loaded with small molecules by integrated processes. *J Biomech* 2007; 40: 80–88.

32. Ho ST and Hutmacher DW. A comparison of micro CT with other techniques used in the characterization of scaffolds. *Biomaterials* 2006; 27: 1362–1376.
33. Grulke EA. Solubility parameter values. In: Brandrup EH, Immergut EA (eds) *Polymer handbook*, 4th ed. New York: Wiley, 1999, p.675.
34. Yang F, Qu X, Cui W, Bei J, Yu F, Lu S, et al. Manufacturing and morphology structure of polylactide-type microtubules orientation-structured scaffolds. *Biomaterials* 2006; 27: 4923–4933.
35. Nam YS and Park TG. Porous biodegradable polymeric scaffolds prepared by thermally induced phase separation. *J Biomed Mater Res* 1999; 47: 8–17.
36. Tu C, Cai Q, Yang J, Wan Y, Bei J and Wang S. The fabrication and characterization of poly(lactic acid) scaffolds for tissue engineering by improved solid-liquid phase separation. *Polym Adv Technol* 2003; 14: 565–573.
37. Graham PD and McHugh AJ. Kinetics of thermally induced phase separation in a crystallizable polymer solution. *Macromolecules* 1998; 31: 2565–2568.
38. Huang JC, Lin KT and Deanin RD. Three-dimensional solubility parameters of poly(ε′-caprolactone). *J Appl Polym Sci* 2006; 100: 2002–2009.
39. Ma PX, Zhang R, Xiao G and Franceschi R. Engineering new bone tissue in vitro on highly porous poly(alpha-hydroxyl acids)/hydroxyapatite composite scaffolds. *J Biomed Mater Res* 2001; 54: 284–293.
40. Yang F, Qu X, Cui W, Bei J, Yu F, Lu S, et al. Manufacturing and morphology structure of polylactide-type microtubules orientation-structured scaffolds. *Biomaterials* 2006; 27: 4923–4933.
41. Song SW and Torkelson JM. Coarsening effects on microstructure formation in isopycnic polymer solutions and membranes produced via thermally induced phase separation. *Macromolecules* 1994; 27: 6389–6397.
42. Burghardt WR. Phase diagrams for binary polymer systems exhibiting both crystallization and limited liquid-liquid miscibility. *Macromolecules* 1989; 22: 2482–2486.
43. Mandoli C, Mecheri B, Forte G, Pagliari F, Pagliari S, Carotenuto F, et al. Thick soft tissue reconstruction on highly perfusive biodegradable scaffolds. *Macromol Biosci* 2010; 10: 127–138.
44. Schugens C, Maquet V, Grandfils C, Jerome R and Teyssie P. Biodegradable and macroporous polylactide implants for cell transplantation: 1. Preparation of macroporous polylactide supports by solid-liquid phase separation. *Polymer* 1996; 37: 1027–1038.
45. Guarino V, Guaccio A, Netti PA and Ambrosio L. Image processing and fractal box counting: user-assisted method for multi-scale porous scaffold characterization. *J Mater Sci Mater Med* 2010; 21: 3109–3118.